THE JOURNAL OF PHYSICAL CHEMISTRY C
A JOURNAL OF THE AMERICAN CHEMICAL SOCIETY

pubs.acs.org/JPCC

Article

From Bulk to Surface: A Raman Spectroscopic Analysis of Solvation Structures in Concentrated Acetonitrile Electrolytes for Li−O_2 Batteries

Koki Kannari, Aimin Ge, Chengyang Xu, Ken-ichi Inoue, and Shen Ye*

Cite This: *J. Phys. Chem. C* 2024, 128, 20148−20155

Read Online

ACCESS | Metrics & More | Article Recommendations | Supporting Information

ABSTRACT: Recent studies indicate that concentrated electrolyte solutions can enhance the stability of organic solvents during the charge/discharge processes in lithium−oxygen (Li−O_2) batteries. However, the effects of electrolyte concentration on the solvation structures of lithium ions (Li-ions) at the electrode surface and their implications for oxygen reduction and evolution reactions (ORR/OER) remain poorly understood. In this study, we investigate the solvation structures of Li-ions in bulk solutions and on a gold electrode surface at various concentrations of acetonitrile (CH_3CN) and lithium bis(trifluoromethanesulfonyl)-imide (LiTFSI) electrolytes, using in situ Raman and surface-enhanced Raman spectroscopy. Our findings show that increasing electrolyte concentration decreases the number of free CH_3CN molecules, significantly altering solvation structures at the electrode surface. Decomposed CH_3CN species predominate the gold electrode surface, while the irreversible side reactions are suppressed in highly concentrated electrolytes. This research highlights the importance of electrolyte concentration in optimizing solvation structures and enhancing the electrolyte stability of Li−O_2 batteries.

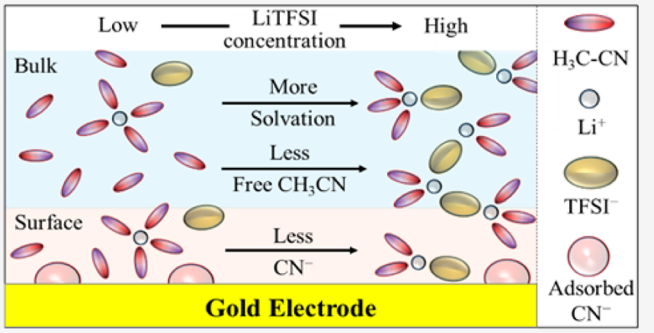

INTRODUCTION

Li−O_2 batteries have garnered significant research interest due to their high theoretical specific energy density, surpassing traditional Li-ion batteries.[1−4] While Li−O_2 batteries hold promise as next-generation secondary batteries,[5] they face several challenges in practical applications. A critical factor for improvement lies in optimizing the aprotic organic electrolyte solutions used. It has been reported that the organic electrolytes can decompose under operational conditions, either through electrochemical oxidation during charging or chemical reactions with intermediates formed during discharging on the cathode surface.[6−10] Consequently, considerable efforts have been made toward developing stable aprotic organic solvents.[11−13]

Li-ion, which has a small ionic radius and thus very high charge density compared to its counteranions, is strongly solvated by the solvent in the organic electrolyte solutions, which can significantly affect the stability of the solvent. One Li-ion is typically solvated by four solvent molecules in the organic electrolyte solution.[14−17] For ionic conductivity and cost considerations, the electrolyte solutions used in the Li-ion batteries have been generally optimized around 1.0 M.[18] For instance, a 1.0 M LiTFSI/CH_3CN solution has a molar ratio of approximately 1 Li-ion to 20 CH_3CN molecules, leading to many uncoordinated (free) solvents. As the concentration increases to a molar ratio of Li-ion and CH_3CN lower than 1:4, the number of CH_3CN molecules becomes insufficient to maintain the four-coordination solvation state, resulting in no free CH_3CN available, with some anions ($TFSI^-$) also participating in the first solvation shell. Therefore, increasing electrolyte concentration significantly alters the coordination state of solvents around Li-ions, which in turn influences the physical properties of electrolytes.

While the ionic conductivity of Li-ion typically decreases in concentrated electrolytes, the performance of both Li-ion[19−22] and Li−O_2 batteries can be enhanced, especially at very high concentrations.[14,23−26] Highly concentrated electrolytes can improve the formation of the solid electrolyte interphase (SEI) and the reversibility of lithium dissolution/deposition reactions on the anode surface of Li−O_2 batteries.[27−30] For example, CH_3CN is known to react rapidly with lithium metal, rendering it unsuitable for lithium batteries.[31] However, Yamada et al. reported that the side reactions between CH_3CN and lithium could be significantly suppressed in the highly concentrated LiTFSA/CH_3CN electrolyte.[19] This

Received: October 3, 2024
Revised: October 30, 2024
Accepted: November 4, 2024
Published: November 15, 2024

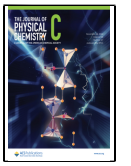

https://doi.org/10.1021/acs.jpcc.4c06709
J. Phys. Chem. C 2024, 128, 20148−20155

highly concentrated solution also shows favorable transport properties for Li-ions, a wide electrochemical window, low volatility, and reduced flammability. Liu et al. reported that a higher concentration of LiTFSI/1,2-dimethoxyethane (DME) electrolytes could improve the discharge/charge performance and cyclability of the Li−O_2 battery cathode.[26] Tatara et al. revealed that the formation of soluble intermediates on the cathode surface decreases in the highly concentrated LiTFSA/DMSO solutions by controlling the reaction pathway.[14] Wang et al. found that, as LiTFSI/DMSO electrolyte concentrations increase, $TFSI^-$ anions start to bind with Li-ions, displacing DMSO from the adsorption layer on the gold electrode surface.[15] Recently, they studied oxygen reduction reactions involving varying concentrations of lithium nitrate ($LiNO_3$) in DMSO and reported that superoxide (O_2^-) is increasingly adsorbed on the electrode surface, facilitating further electrochemical reduction to lithium peroxide (Li_2O_2) at higher $LiNO_3$ concentrations.[32] Sayama et al. reported that free or solvating CH_3CN molecules are present even near the platinum electrode, with solvent degradation being suppressed at high concentrations, as observed by sum frequency generation (SFG) measurements.[33,34]

However, the precise effects of concentrated electrolytes on the reaction mechanisms and stability of solvents during the oxygen reduction reaction (ORR, discharge) and oxygen evolution reaction (OER, charge) in Li−O_2 batteries remain unclear. In the present study, we investigated the coordination state of CH_3CN in bulk solutions and on the electrode surface at different Li-salt concentrations by Raman spectroscopy and surface-enhanced Raman spectroscopy (SERS), respectively. Most CH_3CN molecules are associated with Li-ions at high concentrations in bulk solutions and at the electrode surface. Notably, decomposed species from CH_3CN predominantly cover the gold electrode surface, while the irreversible side reactions are suppressed in highly concentrated electrolytes. Furthermore, *in situ* SERS measurements evaluated the adsorption and solvation structures of CH_3CN on the gold electrode surface during the discharge and charge processes in Li−O_2 batteries.

EXPERIMENTAL SECTION

Sample Preparation. Acetonitrile (CH_3CN, > 99.5%) and lithium bis(trifluoromethane sulfonyl)imide (LiTFSI, > 98%) were purchased from FUJIFILM Wako Pure Chemical Corporation. Before use, CH_3CN was further dried with molecular sieves (4 Å), resulting in a water residue of <5 ppm. LiTFSI was dried at 150 °C under vacuum for over 48 h.

As shown in Table 1, several concentrations of LiTFSI/CH_3CN solutions were prepared for this study. These solutions' molar concentrations (molarity) were calculated from the Li-salt mole normalized by the solution volume in a volumetric flask. Both the molarity and molal concentrations (molality) are given in Table 1. The electrolyte solutions were prepared and stored in an argon-filled glovebox (MIKROUNA, O_2 < 0.5 ppm, water <0.01 ppm). For the electrochemical measurements, oxygen was purged to the solutions in an O_2-filled glovebox (UNICO, water <0.5 ppm). The water content in these electrolyte solutions was typically below 30 ppm, as measured by a Karl Fischer moisture titrator (MKC-710, Kyoto Electronics). However, the water content slightly increased during the in situ measurements due to the laboratory atmosphere.

Table 1. Molar Concentrations of LiTFSI/CH_3CN Solutions Used in This Study, Corresponding Molar Ratio and Molal Concentration

Molar Concentration (M)	0.1	0.9	1.6	2.3	4.2
Molar ratio (LiTFSI:CH_3CN)	1:115	1:18	1:9	1:5.5	1:2
Molal Concentration (mol/kg)	0.212	1.35	2.71	4.43	12.2

Raman Measurements. The Raman spectra were collected using a confocal Raman microscope (XploRA plus, HORIBA) with an excitation wavelength of 785 nm (ca. 4 mW) and a 20X objective lens (NA = 0.45, Olympus). A diffraction grating of 1200 lines/mm (corresponding to a spectral resolution of 1.3 cm^{-1}) was used for bulk solution measurements. The solutions were in a cell separated by two calcium fluoride (CaF_2) windows with a 1 mm spacer. The integration time for each spectrum was 60 s (15 s × 4).

In situ SERS measurements were carried out on a SERS-active gold electrode.[35,36] The gold thin-film electrode was fabricated by the sputtering on a polished stainless-steel plate, using Auto Fine Coater (JFC-1300, JEOL) in an argon-plasma environment (10 Pa and 40 mA current) for 300 s. Details for the preparation have been reported elsewhere.[37] The surface of the sputtered thin gold film was uniform, comprising small gold islands of roughly 50 nm dimensions (see Figure S1). The gold electrode demonstrated excellent and well-reproducible SERS activity and electrochemical stability.

A homemade SERS cell was used in the study (Figure S1).[6] The thickness of the electrolyte solution between the optical window and electrode surface during in situ SERS measurement was maintained at about 1 mm. A diffraction grating of 600 lines/mm (corresponding to a spectral resolution of ca. 3.0 cm^{-1}) was used for the SERS measurements on the gold electrode surface. The typical integration time for each SERS spectrum was 20 s (10 s × 2).

Electrochemical Measurements. The electrochemical measurements were carried out in the SERS cell. Due to the low stability of lithium against CH_3CN at a lower electrolyte concentration, lithium iron(II) phosphate ($LiFePO_4$, LFP) was employed as both the reference and counter electrode when the LiTFSI concentrations were below 2.5 M based on experience. Lithium foils were used as the reference and counter electrode when the LiTFSI concentration exceeded this threshold. All electrode potentials in the study were referred to Li^+/Li. Electrochemical measurements were carried out with a Polarization Unit PS-07 (TOHO Technical research). Cyclic voltammetry (CV) was performed at a sweep rate of 2 mV/s. A potential window of 40 mV corresponds to a simultaneously recorded SERS spectrum. The current and potential outputs from the potentiostat were recorded by a multifunction data acquisition module (USB-6211, National Instruments) controlled by LabVIEW.

RESULT AND DISCUSSION

Solvation Structure in CH_3CN/LiTFSI Solution. Figure 1a shows the Raman spectra of LiTFSI/CH_3CN solutions at various concentrations (0−4.2 M) within the spectral range of 2050 and 2350 cm^{-1} (also see Raman spectra in a wide region between 400 and 2500 cm^{-1} in Figure S2). The spectrum of pure CH_3CN (0 M) gives two distinct peaks: one at 2252 cm^{-1} (denoted as Peak 1) and another weaker one at 2293 cm^{-1} (Peak 2). Peak 1 at 2252 cm^{-1} can be assigned to the C≡N stretching mode of CH_3CN, while Peak 2 at 2293 cm^{-1}

https://doi.org/10.1021/acs.jpcc.4c06709
J. Phys. Chem. C 2024, 128, 20148−20155

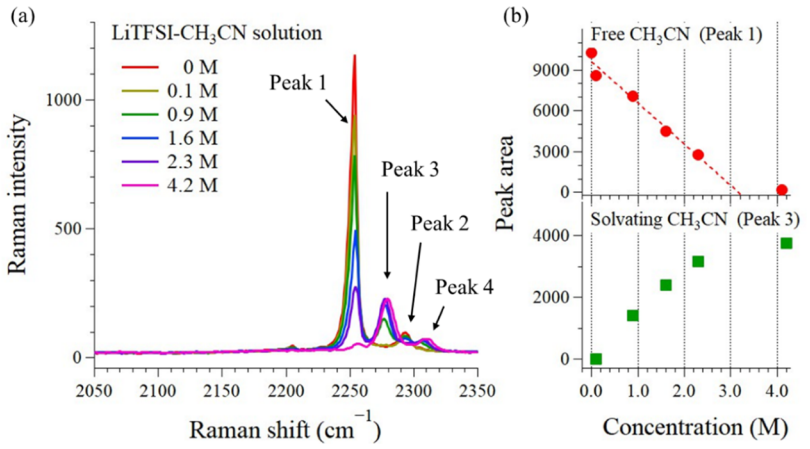

Figure 1. (a) Raman spectra in various concentrations of LiTFSI/CH_3CN solutions in the region of CN stretching. (b) The peak are changes of free CH_3CN (peak 1) and Li^+ -solvating CH_3CN (peak 3). The red dashed line indicates the decrease in the peak area of free CH_3CN determined by fitting using five points (0 M ∼ 2.3 M).

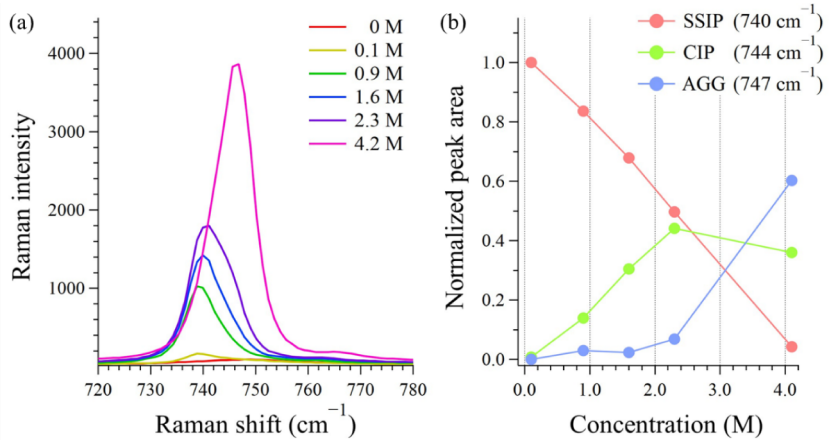

Figure 2. (a) Raman spectra in various concentrations of LiTFSI/CH_3CN solutions in the region of S−N−S streching for $TFSI^-$. (b) Normalized peak areas of $TFSI^-$ anions in SSIP, CIP, and AGG states. Each peak is normalized by the summation of these 3 peak areas.

can be attributed to the combination mode of the CH_3 deformation mode and C−C stretching mode of CH_3CN.[38] As the concentration of LiTFSI increases, the intensities of both peaks gradually decrease, and two new peaks emerge at 2277 cm^{-1} (Peak 3) and 2308 cm^{-1} (Peak 4). Based on the previous studies,[19] Peak 3 at 2277 cm^{-1} can be assigned to the C≡N stretching mode of CH_3CN in coordination with the Li-ion (denoted as $H_3C-C{\equiv}N{:}Li^+$). Similarly, Peak 4 at 2308 cm^{-1} corresponds to the combination mode of CH_3 deformation and C−C stretching for the CH_3CN solvating with the Li-ion.[39] The two pairs of peaks correspond to Raman modes of free (Peak1 and 2) and Li^+-solvating CH_3CN molecules (Peak 3 and 4), respectively. Notably, the peak shifts of CH_3CN arise from coordination to Li-ion, with variations in coordination number (i.e., 3- or 4-coordination) contributing minimally to these shifts.

To quantitatively assess the concentration dependence, the Raman spectra were fitted based on the Lorentz function for the four identified modes (see Figure S3). Figure 1b shows the peak areas of the fitted components for the C≡N stretching mode of free (red circles, Peak 1) and solvating CH_3CN (green blocks, Peak 3) as a function of concentration. As concentration increases, the intensity of Peak 1 decreases while that of Peak 3 increases. Notably, both trends are more pronounced in lower concentration ranges but taper off at higher concentrations. Based on a linear extrapolation, it is predicted that free CH_3CN will cease to be detectable beyond 3.2 M. Yamada et al. reported that 3.0 M LiTFSI/CH_3CN solution has a molar ratio of Li-ion and CH_3CN is 1:3.5.[19] Therefore, one expects that the first solvation shell, where the solvents are directly coordinated to Li-ion, is formed by three to four CH_3CN molecules per Li-ion.

Figure 2a shows Raman spectra for the $TFSI^-$ anion between 720 and 780 cm^{-1}. A broad peak around 740 cm^{-1} in 0.1 M LiTFSI/CH_3CN solution can be assigned to the S−N−S symmetric stretching of the $TFSI^-$ anion.[15] As concentration increases, the peak position shifts to higher frequencies, and the peak width looks broader. Two new components are devoluted around 744 and 747 cm^{-1} (detailed deconvoluted results are shown in Figure S4). As a hard acid, Li-ion is more strongly solvated by CH_3CN (donor number (DN) = 4) than $TFSI^-$ anion (DN = 7−10).[40−42] Thus, CH_3CN predominantly coordinates with Li-ions at lower concentrations, while $TFSI^-$ anions are located outside the solvation shell, resulting in a solvent-separated ion pair (SSIP) state. As the concentration increases, $TFSI^-$ anions can interact with Li-ion to participate in the solvation shell. Each $TFSI^-$ anion can be associated with one and two (or more) Li-ion, denoting contact ion pairs (CIP) and aggregates (AGG), respectively. The peak at 740 cm^{-1} can be attributed to the $TFSI^-$ anion in

https://doi.org/10.1021/acs.jpcc.4c06709
J. Phys. Chem. C 2024, 128, 20148−20155

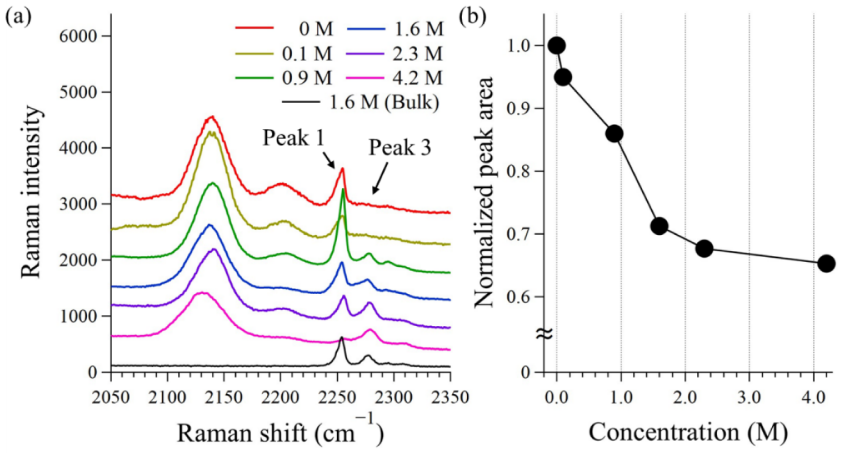

Figure 3. (a) SERS spectra collected on Au surface in various concentrations of LiTFSI/CH_3CN solutions. (b) Normalized peak areas of adsorbed CN^- peak at 2137 cm^{-1} in various concentrations. The peak areas were normalized by the peak area of adsorbed CN^- at 0 M.

SSIP, while peaks at 744 and 747 cm^{-1} can be associated with CIP and AGG, respectively.[19,43]

The results of the quantitative devolution analysis are summarized in Figure 2b (solid traces in Figure 2b are only for eye guidance). When LiTFSI concentration is below 0.9 M, $TFSI^-$ anions are mainly present in the SSIP state. At 2.3 M, $TFSI^-$ anions are predominantly in SSIP and CIP states. At 3.2 M, most $TFSI^-$ anions are involved in the solvation structure as CIP state. At this concentration, a possible first solvation shell in the bulk solution is expected to be formed in a ratio of Li^+: CH_3CN: $TFSI^-$ = 1:4:0 or 1:3:1. When concentration becomes even higher, the first solvation shell in the bulk will contain more structure of CIP and AGG, i.e., more Li-ions will associate with the $TFSI^-$ anions. The present results are generally consistent with previous reports.[19]

Solvation Structure on the Gold Electrode. We further investigated the solvation state on the electrode surface in various concentrations of CH_3CN-based electrolytes (0−4.2 M) using SERS measurement (Figure 3a, 2050−2350 cm^{-1}). For comparison, a Raman spectrum from a 1.6 M LiTFSI/CH_3CN bulk solution is also presented at the bottom of the figure (black trace, Figure 3a). One can see that the spectral profile on the gold electrode surface is quite different from that of the bulk solutions.

First, a SERS peak was observed at 2137 cm^{-1} in pure CH_3CN on the gold surface, which was also observed in other concentrations in the SERS measurements (Figure 3a), but it was absent in the Raman spectra for the bulk solutions (Figure 1a). It is reasonable to attribute it to an adsorbed species exclusive to the gold electrode surface. A similar peak has been reported in the CH_3CN-based solutions, although their origins are still debated.[44,45] Some researchers assigned it to the CN stretching mode of CH_3CN chemically adsorbed on the gold surface.[46] Others attributed it to adsorbed CN^- from the decomposition product of CH_3CN under light irradiation or electrochemical potential control.[44,47−49] Dederichs et al. demonstrated that the CN^- species can be generated by dissociating CH_3CN after cooling the annealed Pt electrode above an aqueous solution of CH_3CN.[50] In the present study, the peak at 2137 cm^{-1} is assigned to adsorbed CN^- from the CH_3CN decomposition without potential control. Another SERS peak around 2200 cm^{-1} is derived from CN^- in different adsorbed states.[44,51−53] The decomposition on a gold electrode surface in a CH_3CN-based solution seems unavoidable.

The peak position for the adsorbed CN^- species irregularly changes with concentration (Figure 3a), and its intensity decreases with concentration (Figure 3b). The adsorbed CN^- species' peak intensity (peak area) decreases with the concentration of LiTFSI/CH_3CN electrolyte solutions (Figure 3b), while the peak position irregularly changes with concentration. The peak intensity for the adsorbed CN^- species in the 4.2 M solution dropped ca. 30% compared to the 0.1 M with a red shift of the peak frequency to 2130 cm^{-1}. The peak frequency changed slightly with the position on the sample surface, especially in the highly concentrated solutions. We only focus on the peak intensity (peak area, Figure 3b), which is proportion to the molecule numbers. The present observations demonstrate that the highly concentrated electrolytes partially suppress the CH_3CN decomposition on the gold electrode surface.

Second, two SERS peaks at 2254 and 2278 cm^{-1} are observed on the gold electrode surface in 1.6 M LiTFSI/CH_3CN, similar to the C≡N stretching mode of free and Li^+-solvating solvents in bulk solution (Peaks 1 and 3, in Figure 3a). The peak positions and intensities change with concentration and can be assigned to the free CH_3CN and Li^+-solvating CH_3CN adsorbed on the gold electrode surface. The SERS peaks corresponding to Peak 2 and 4 in the bulk solution are weak due to low intensity. On the other hand, since a large amount of solvent and LiTFSI salt are present in the bulk solution, these SERS peaks also contain some contributions from the bulk solution, even if we have a significant enhancement factor on the SERS signal.

The solvation shells on the electrode surface are expected to differ from those in the bulk solution due to the interaction with the electrode surface. The spectral fitting shows that the SERS peak at 2254 cm^{-1} on the gold electrode surface shows a full width at half-maximum (fwhm) of 8.6 cm^{-1}, wider than the fwhm of 6.7 cm^{-1} observed for free CH_3CN in the bulk solution. Furthermore, Table 2 summarizes the intensity ratio of the Li^+-solvating CH_3CN peak (Peak 3) to the free CH_3CN peak (Peak 1) on the gold electrode surface and in bulk solution in different concentrations based on the results in Figures 1 and 3. The present results show that the solvated and free CH_3CN ratios on the electrode surface are always lower than those of the bulk solution. In other words, a comparatively larger number of free CH_3CN are present on the electrode−electrolyte interface in the same electrolyte

https://doi.org/10.1021/acs.jpcc.4c06709
J. Phys. Chem. C 2024, 128, 20148−20155

Table 2. Relative Peak Intensities of Li^+-Solvating CH_3CN Peak (Peak 3) to the Free CH_3CN Peak (Peak 1) in Bulk Solution and on the Gold Electrode Surface in Various Concentrations of LiTFSI/CH_3CN Solutions

Molar Concentration (M)		0.9	1.6	2.3	4.2
Relative Intensity (Peak 3/Peak 1)	Bulk	0.23	0.78	1.2	19.8
	Electrode surface	0.20	0.55	1.1	3.8

solution. Increasing the concentration also causes a rise in Li^+-solvating CH_3CN at the interface. Therefore, it is insufficient to discuss the electrolyte solution's stability solely based on the bulk properties.

Yang et al. previously reported that solvation numbers decreased on the SERS-active gold nanogap substrate interface based on discussions of peak intensities in the IR, Raman, and SERS spectra.[54] They found that the solvation number in several concentrations of $LiPF_6$ in EC/DEC solutions is lower at these interfaces than in bulk solution because its nanostructure limits the size of the solvation shells, especially the second solvation shell.

Figure 4 shows a schematic model for the solvation structure in the bulk solution and on the electrode surface. In the bulk

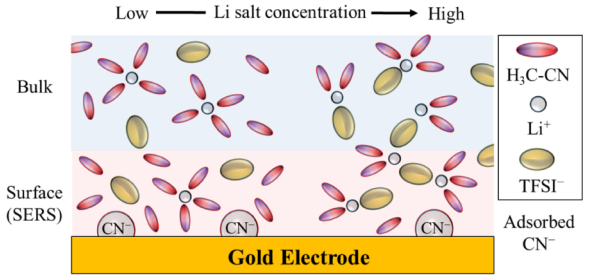

Figure 4. Schematics of the solvation structure in various concentrations of LiTFSI/CH_3CN solutions in bulk and on the gold electrode surface.

solution, the solvation structure of Li-ion varies with concentration. As the concentration increases, more CH_3CN molecules associate with Li-ion, and no free CH_3CN solvent exists at a concentration higher than 3.2 M. In addition, $TFSI^-$ anions become incorporated into the solvation shells in a CIP state with concentration increase, ultimately forming an AGG state of $TFSI^-$ anions. Highly concentrated electrolytes exhibit unique properties, with the vast majority of solvents coordinated to Li-ions and the increased presence of $TFSI^-$ anions.

On the other hand, the gold electrode surface is covered with CN^- species from CH_3CN decomposition. In highly concentrated solutions, the amount of adsorbed CN^- is reduced due to enhanced solvent stability and the formation of solvation structures. Furthermore, we found that more free CH_3CN solvents are present on the gold electrode surface than in the bulk solution in all solutions (Table 2).

Concentration Effect and Surface Solvation Structure Changes in ORR/OER. Figure 5 shows CV results (sweep rate, 2 mV/s) during ORR/OER in three concentrations of CH_3CN-based solutions (0.1, 1.6, and 4.2 M), all saturated with O_2. During the negative-going potential sweep from the open circuit potential (OCP, ca. 3.1 V), a reduction peak corresponding to ORR ($O_2 + 2\ Li^+ + 2\ e^- \rightarrow Li_2O_2$) was observed. The small ORR overpotential and the high ORR capacity were found in the 1.6 M solution, likely due to the higher ionic conductivity of the 1.6 M LiTFSI-CH_3CN solution. In contrast, the ORR peak in the 4.2 M solution shifted to a more negative potential with a smaller reduction current, possibly influenced by the high viscosity and low diffusion rate in highly concentrated solutions.[18] As the potential was swept in the positive direction for OER ($Li_2O_2 \rightarrow O_2 + 2\ Li^+ + 2\ e^-$), broad anodic waves were observed in 0.1 and 1.6 M solutions, which could be attributed to side reactions, such as solvent and salt decomposition. However, in the 4.2 M solution, a single oxidation peak at 3.1 V appeared with the minimal anodic current in the more positive potential region, implying fewer side reactions in the highly concentrated electrolytes.

In situ SERS measurements were employed to investigate the structural information on the electrode surface during the discharge/charge processes. Figure 5b shows SERS spectra (700−940 cm^{-1}; see Figure S5 for wide spectra at different potentials) in the ORR potential region at 2.4 V. A Raman spectrum of 1.6 M bulk solution is shown in the same figure as a reference (black trace, Figure 5b). In addition to the peaks

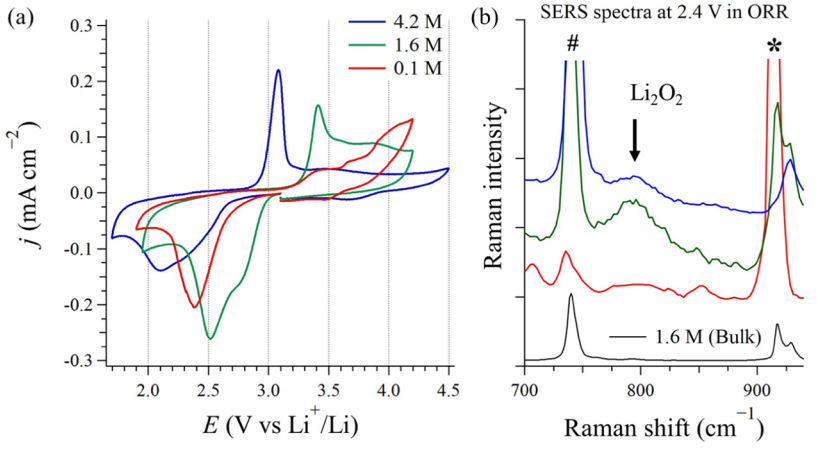

Figure 5. (a) CV observed in 0.1 M (red), 1.6 M (green), and 4.2 M (blue) LiTFSI/CH_3CN solutions. The scan rate was 2 m V/s. (b) *In situ* SERS spectra were collected at 2.4 V during ORR (first negative scan) in each solution. A peak of Li_2O_2 appears at 790 cm^{-1}, marked by an arrow. *and # indicate the peak derived from CH_3CN and $TFSI^-$, respectively.

https://doi.org/10.1021/acs.jpcc.4c06709
J. Phys. Chem. C 2024, 128, 20148−20155

from CH_3CN solvent and $TFSI^-$ anions, a new SERS band can be identified at 790 cm^{-1}. Based on previous studies,[37,41,55,56] this peak can be assigned to the O−O stretching mode of Li_2O_2 on the electrode surface. Based on our experiences, getting a reproducible SERS band for the Li_2O_2 with good S/N in 0.1 M solution during the ORR proved challenging. However, this task was significantly easier in a concentrated CH_3CN-based solution (Figure 5b), indicating that the higher stability of CH_3CN in the concentrated electrolytes promotes the Li_2O_2 formation, likely due to fewer side reactions.

Figure 6 compares SERS spectra at OCP, the negative potential limit of ORR, and the positive potential limit of OER

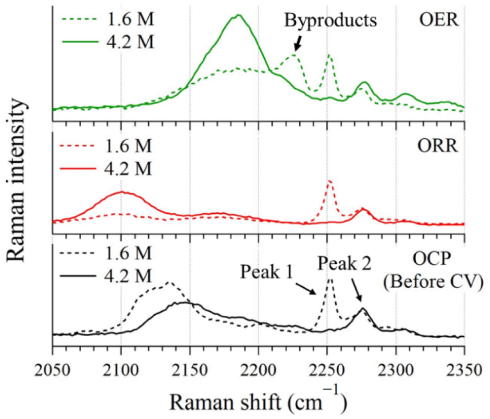

Figure 6. Comparing SERS spectra collected at OCP (black), the negative potential limit of ORR (red trace), and the positive potential limit of OER (green) in 1.6 M (dashed) and 4.2 M solutions(solid).

in 1.6 and 4.2 M solutions. As mentioned, the SERS band at 2130 cm^{-1} at OCP is assigned to the adsorbed CN^- species on the gold electrode surface from CH_3CN decomposition. Based on the electrochemical Stark effect, the peak position can shift to lower or higher frequencies at negative or positive potential regions.[49] The adsorbed CN^- species can also be influenced by associated ions or solvent molecules (i.e., $CN^-\cdots Li^+$ and $CN^-\cdots CH_3CN$).[49,53,57]

In the 1.6 M solution, the new SERS peak was observed at 2227 cm^{-1} after OER (denoted by an arrow in the spectrum). This peak may be attributed to byproducts from the side reactions between CN^- and OER intermediates such as superoxide (O_2^-) or singlet oxygen. It has been reported that the peak position of CN stretching mode in Au-CNO^- is at 2223 cm^{-1}.[51] This byproduct may indicate the formation of CNO species at high charging overpotential region during OER. This species was not observed in a highly concentrated solution (4.2 M), implying that the side reactions were suppressed due to the enhanced stability of Li^+-solvating CH_3CN on the electrode surface and the reduced overpotential for OER.

Moreover, free and solvating CH_3CN species (Peak 1 and 3) are observed in 1.6 and 4.2 M solutions. After ORR and OER, the intensities of free and solvating CH_3CN were lower than at OCP. These irreversible intensity changes suggest that residual byproducts may persist on the surface after the ORR/OER cycle. Furthermore, in the 1.6 M solution, the intensity ratio of solvating to free molecules slightly decreases after the ORR/OER cycle (before: 0.80, After: 0.71). This result suggests that the proportion of Li^+-solvating CH_3CN diminishes during the ORR/OER, potentially accelerating side reactions.

As the concentration increases, free CH_3CN decreases while solvating CH_3CN increases, improving solvent stability. The free CH_3CN molecules, especially those on the electrode surface, are prone to side reactions. Therefore, understanding the structure and solvation states on the electrode surface is crucial. The higher proportion of free CH_3CN on the electrode surface in the 1.6 M solution results in lower stability and higher irreversibility than the 4.2 M solution, which can be attributed to the fewer side reactions in the more concentrated solution. Also, $TFSI^-$-based species should be the surface layer, especially in highly concentrated solutions, as shown in the previous study.[34] Further investigations are necessary to determine how this stability affects the battery cycling performance and clarify the effect of $TFSI^-$ anions on electrode surface coverage.

CONCLUSION

In summary, we have investigated the concentration dependence of the solvation structure and the ORR/OER behaviors in the CH_3CN-based electrolyte solutions by in situ Raman and SERS techniques. The formation of solvation structures evolves with increasing concentration. In highly concentrated electrolytes, almost no free CH_3CN molecules are present in the bulk solution. Instead, adsorbed CN^- species from the decomposition of CH_3CN dominate the gold electrode surface. The amount of adsorbed CN^- decreases with increasing concentration, significantly altering the electrode surface's solvation state. Irreversible side reactions of CH_3CN solvents during ORR/OER can be partially mitigated in highly concentrated electrolytes. The stability of the electrolyte solution on the electrode surface can be controlled by optimizing the electrolyte concentration.

ASSOCIATED CONTENT

Supporting Information

The Supporting Information is available free of charge at https://pubs.acs.org/doi/10.1021/acs.jpcc.4c06709.

Cell information, Raman spectra of electrolyte solution with a wide frequency range(PDF)

AUTHOR INFORMATION

Corresponding Author

Shen Ye − *Department of Chemistry, Graduate School of Science, Tohoku University, Sendai 980-8578, Japan;* orcid.org/0000-0002-0090-7855; Email: ye.shen@tohoku.ac.jp

Authors

Koki Kannari − *Department of Chemistry, Graduate School of Science, Tohoku University, Sendai 980-8578, Japan*

Aimin Ge − *Center for Advanced Low-dimension Materials, Donghua University, Shanghai 201620, P. R. China;* orcid.org/0000-0003-0127-3193

Chengyang Xu − *Department of Chemistry, Graduate School of Science, Tohoku University, Sendai 980-8578, Japan*

Ken-ichi Inoue − *Department of Chemistry, Graduate School of Science, Tohoku University, Sendai 980-8578, Japan;* orcid.org/0000-0001-6237-6618

Complete contact information is available at: https://pubs.acs.org/10.1021/acs.jpcc.4c06709

Notes

The authors declare no competing financial interest.

■ ACKNOWLEDGMENTS

Shen Ye acknowledges support from the Advanced Low Carbon Technology Research and Development Program (ALCA), specially promoted research for innovative next-generation batteries (SPRING), and the ASPIRE (JPMJAP2309), from the Japan Science and Technology Agency (JST). Koki Kannari acknowledges a fellowship (DC1) from JSPS and support from GP-MS at Tohoku University. Aimin Ge acknowledges the support provided by the Natural Science Foundation of Shanghai (Grant No. 23ZR1400300).

■ REFERENCES

(1) Kwak, W.-J.; Rosy; Sharon, D.; Xia, C.; Kim, H.; Johnson, L. R.; Bruce, P. G.; Nazar, L. F.; Sun, Y.-K.; Frimer, A. A.; Noked, M.; Freunberger, S. A.; Aurbach, D. Lithium−Oxygen Batteries and Related Systems: Potential, Status, and Future. *Chem. Rev.* **2020**, *120*, 6626−6683.

(2) Ma, L.; Yu, T.; Tzoganakis, E.; Amine, K.; Wu, T.; Chen, Z.; Lu, J. Fundamental Understanding and Material Challenges in Rechargeable Nonaqueous Li−O_2 Batteries: Recent Progress and Perspective. *Adv. Energy Mater.* **2018**, *8*, 1800348.

(3) Luntz, A. C.; McCloskey, B. D. Nonaqueous Li−air batteries: a status report. *Chem. Rev.* **2014**, *114*, 11721−11750.

(4) Zhang, X.; Wang, X.-G.; Xie, Z.; Zhou, Z. Recent progress in rechargeable alkali metal−air batteries. *Green Energy Environ.* **2016**, *1*, 4−17.

(5) Ue, M.; Sakaushi, K.; Uosaki, K. Basic knowledge in battery research bridging the gap between academia and industry. *Mater. Horiz.* **2020**, *7*, 1937−1954.

(6) Peng, Q.; Qiao, Y.; Kannari, K.; Ge, A.; Inoue, K.; Ye, S. In Situ Spectroscopic Investigations of Electrochemical Oxygen Reduction and Evolution Reactions in the Cyclic Carbonate Electrolyte Solutions. *J. Phys. Chem. C* **2020**, *124*, 15781−15792.

(7) Ue, M.; Asahina, H.; Matsuda, S.; Uosaki, K. Material balance in the O_2 electrode of Li−O_2 cells with a porous carbon electrode and TEGDME-based electrolytes. *RSC Adv.* **2020**, *10*, 42971−42982.

(8) Schroeder, M. A.; Kumar, N.; Pearse, A. J.; Liu, C.; Lee, S. B.; Rubloff, G. W.; Leung, K.; Noked, M. DMSO−Li_2O_2 interface in the rechargeable Li−O_2 battery cathode: theoretical and experimental perspectives on stability. *ACS Appl. Mater. Interfaces* **2015**, *7*, 11402−11411.

(9) Ge, A.; Nagai, R.; Nemoto, K.; Li, B.; Kannari, K.; Inoue, K.; Ye, S. Unraveling the solvent stability on the cathode surface of Li−O_2 batteries by using in situ vibrational spectroscopies. *Faraday Discuss.* **2024**, *248*, 119−133.

(10) Ge, A.; Inoue, K.; Ye, S. Probing the electrode−solution interfaces in rechargeable batteries by sum-frequency generation spectroscopy. *J. Chem. Phys.* **2020**, *153*, 170902.

(11) Christy, M.; Arul, A.; Zahoor, A.; Moon, K. U.; Oh, M. Y.; Stephan, A. M.; Nahm, K. S. Role of solvents on the oxygen reduction and evolution of rechargeable Li-O_2 battery. *J. Power Sources* **2017**, *342*, 825−835.

(12) Nishioka, K.; Tanaka, M.; Fujimoto, H.; Amaya, T.; Ogoshi, S.; Tobisu, M.; Nakanishi, S. Overlooked Factors Required for Electrolyte Solvents in Li−O_2 Batteries: Capabilities of Quenching $^1O_2$ and Forming Highly-Decomposable Li_2O_2. *Angew. Chem., Int. Ed.* **2022**, *61*, No. e202112769.

(13) Huang, Z.; Meng, J.; Zhang, W.; Shen, Y.; Huang, Y. 1,3-Dimethyl-2-imidazolidinone: an ideal electrolyte solvent for high-performance Li−O_2 battery with pretreated Li anode. *Sci. Bull.* **2022**, *67*, 141−150.

(14) Tatara, R.; Kwabi, D. G.; Batcho, T. P.; Tulodziecki, M.; Watanabe, K.; Kwon, H.-M.; Thomas, M. L.; Ueno, K.; Thompson, C. V.; Dokko, K.; Shao-Horn, Y.; Watanabe, M. Oxygen reduction reaction in highly concentrated electrolyte solutions of lithium bis (trifluoromethanesulfonyl) amide/dimethyl sulfoxide. *J. Phys. Chem. C* **2017**, *121*, 9162−9172.

(15) Wang, L.; Uosaki, K.; Noguchi, H. Effect of Electrolyte Concentration on the Solvation Structure of Gold/LiTFSI-DMSO Solution Interface. *J. Phys. Chem. C* **2020**, *124*, 12381.

(16) Brouillette, D.; Irish, D. E.; Taylor, N. J.; Perron, G.; Odziemkowski, M.; Desnoyers, J. E. Stable solvates in solution of lithium bis (trifluoromethylsulfone) imide in glymes and other aprotic solvents: Phase diagrams, crystallography and Raman spectroscopy. *Phys. Chem. Chem. Phys.* **2002**, *4*, 6063−6071.

(17) Lundin, F.; Aguilera, L.; Hansen, H. W.; Lages, S.; Labrador, A.; Niss, K.; Frick, B.; Matic, A. Structure and dynamics of highly concentrated LiTFSI/acetonitrile electrolytes. *Phys. Chem. Chem. Phys.* **2021**, *23*, 13819−13826.

(18) Ugata, Y.; Tatara, R.; Ueno, K.; Dokko, K.; Watanabe, M. Highly concentrated $LiN(SO_2CF_3)_2$/dinitrile electrolytes: Liquid structures, transport properties, and electrochemistry. *J. Chem. Phys.* **2020**, *152*, 104502.

(19) Yamada, Y.; Furukawa, K.; Sodeyama, K.; Kikuchi, K.; Yaegashi, M.; Tateyama, Y.; Yamada, A. Unusual stability of acetonitrile-based superconcentrated electrolytes for fast-charging lithium-ion batteries. *J. Am. Chem. Soc.* **2014**, *136*, 5039−5046.

(20) Borodin, O.; Self, J.; Persson, K. A.; Wang, C.; Xu, K. Uncharted waters: super-concentrated electrolytes. *Joule* **2020**, *4*, 69−100.

(21) Zheng, J.; Lochala, J. A.; Kwok, A.; Deng, Z. D.; Xiao, J. Research progress towards understanding the unique interfaces between concentrated electrolytes and electrodes for energy storage applications. *Adv. Sci.* **2017**, *4* (8), 1700032.

(22) Yamada, Y.; Yamada, A. Superconcentrated electrolytes for lithium batteries. *J. Electrochem. Soc.* **2015**, *162*, A2406.

(23) Markus, I. M.; Jones, G.; Garcia, J. M. Investigation of electrolyte concentration effects on the performance of lithium−oxygen batteries. *J. Phys. Chem. C* **2016**, *120*, 5949−5957.

(24) Yoo, E.; Qiao, Y.; Zhou, H. Understanding the effect of the concentration of $LiNO_3$ salt in Li−O_2 batteries. *J. Mater. Chem. A* **2019**, *7*, 18318−18323.

(25) Chen, J.; Chen, C.; Huang, T.; Yu, A. LiTFSI Concentration Optimization in TEGDME Solvent for Lithium−Oxygen Batteries. *ACS Omega* **2019**, *4*, 20708−20714.

(26) Liu, B.; Xu, W.; Yan, P.; Sun, X.; Bowden, M. E.; Read, J.; Qian, J.; Mei, D.; Wang, C. M.; Zhang, J. G. Enhanced cycling stability of rechargeable Li−O_2 batteries using high-concentration electrolytes. *Adv. Funct. Mater.* **2016**, *26*, 605−613.

(27) Ugata, Y.; Tatara, R.; Mandai, T.; Ueno, K.; Watanabe, M.; Dokko, K. Understanding the Reductive Decomposition of Highly Concentrated Li Salt/Sulfolane Electrolytes during Li Deposition and Dissolution. *ACS Appl. Energy Mater.* **2021**, *4*, 1851−1859.

(28) Pranay Reddy, K.; Fischer, P.; Marinaro, M.; Wohlfahrt-Mehrens, M. Improved Li−Metal Cycling Performance in High Concentrated Electrolytes for Li-O_2 Batteries. *ChemElectrochem* **2018**, *5*, 2758−2766.

(29) Qian, J.; Henderson, W. A.; Xu, W.; Bhattacharya, P.; Engelhard, M.; Borodin, O.; Zhang, J.-G. High rate and stable cycling of lithium metal anode. *Nat. Commun.* **2015**, *6*, 6362.

(30) Hu, Y.-S.; Pan, H. Solvation Structures in Electrolyte and the Interfacial Chemistry for Na-Ion Batteries. *ACS Energy Lett.* **2022**, *7*, 4501−4503.

(31) Rupich, M.; Pitts, L.; Abraham, K. Characterization of reactions and products of the discharge and forced overdischarge of Li/SO_2 cells. *J. Electrochem. Soc.* **1982**, *129*, 1857.

(32) Wang, L.; Noguchi, H. Oxygen Reduction Reaction Mechanism in Highly Concentrated Lithium Nitrate-Dimethyl Sulfoxide: Effect of Lithium Nitrate Concentration. *J. Phys. Chem. C* **2022**, *126*, 11457−11467.

(33) Sayama, A.; Nihonyanagi, S.; Ohshima, Y.; Tahara, T. In situ observation of the potential-dependent structure of an electrolyte/

https://doi.org/10.1021/acs.jpcc.4c06709
J. Phys. Chem. C 2024, 128, 20148−20155

electrode interface by heterodyne-detected vibrational sum frequency generation. *Phys. Chem. Chem. Phys.* **2020**, *22*, 2580−2589.
(34) Sayama, A.; Nihonyanagi, S.; Ohshima, Y.; Tahara, T. Origin of Solvent Stabilization at Superconcentrated Electrolyte/Electrode Interfaces Revealed by Heterodyne-Detected Vibrational Sum Frequency Generation Spectroscopy. *J. Phys. Chem. C* **2023**, *127*, 10524−10531.
(35) Han, X.-B.; Kannari, K.; Ye, S. In Situ Surface-enhanced Raman Spectroscopy (SERS) in Li−O_2 Battery Research. *Curr. Opin. Electrochem.* **2019**, *17*, 174.
(36) Ge, A.; Nagai, R.; Xu, C.; Kannari, K.; Peng, B.; Inoue, K.; Morita, A.; Ye, S. Unraveling the Unstable Nature of Tetraglyme-Based Electrolytes toward Superoxide and the Inhibitory Effect of Lithium Ions by Using In Situ Vibrational Spectroscopies. *J. Phys. Chem. C* **2022**, *126*, 2980−2989.
(37) Yu, Q.; Ye, S. In situ study of oxygen reduction in dimethyl sulfoxide (DMSO) solution: a fundamental study for development of the lithium−oxygen battery. *J. Phys. Chem. C* **2015**, *119*, 12236−12250.
(38) Givan, A.; Loewenschuss, A. Inter-and intra-molecular Raman spectrum of matrix-isolated acetonitrile. *J. Mol. Struct.* **1983**, *98*, 231−238.
(39) Xuan, X.; Zhang, H.; Wang, J.; Wang, H. Vibrational spectroscopic and density functional studies on ion solvation and association of lithium tetrafluorobrate in acetonitrile. *J. Phys. Chem. A* **2004**, *108*, 7513−7521.
(40) Gutmann, V.; Gutmann, V. *The donor-acceptor approach to molecular interactions*; Springer, 1978; Vol. *228*.
(41) Johnson, L.; Li, C.; Liu, Z.; Chen, Y.; Freunberger, S. A.; Ashok, P. C.; Praveen, B. B.; Dholakia, K.; Tarascon, J.-M.; Bruce, P. G. The role of LiO_2 solubility in O_2 reduction in aprotic solvents and its consequences for Li−O_2 batteries. *Nat. Chem.* **2014**, *6*, 1091.
(42) Yamagata, M.; Katayama, Y.; Miura, T. Electrochemical behavior of samarium, europium, and ytterbium in hydrophobic room-temperature molten salt systems. *J. Electrochem. Soc.* **2006**, *153*, No. E5.
(43) Seo, D. M.; Borodin, O.; Han, S.-D.; Boyle, P. D.; Henderson, W. A. Electrolyte solvation and ionic association II. Acetonitrile-lithium salt mixtures: highly dissociated salts. *J. Electrochem. Soc.* **2012**, *159*, A1489.
(44) Murray, C. A.; Bodoff, S. Cyanide adsorption on silver and gold overlayers on island films as determined by surface enhanced Raman scattering. *J. Chem. Phys.* **1986**, *85*, 573−584.
(45) Baltruschat, H.; Heitbaum, J. On the potential dependence of the CN stretch frequency on Au electrodes studied by SERS. *J. Electroanal. Chem. Interfacial Electrochem.* **1983**, *157*, 319−326.
(46) Marinković, N. S.; Hecht, M.; Loring, J. S.; Fawcett, W. R. A SNIFTIRS study of the diffuse double layer at single crystal platinum electrodes in acetonitrile. *Electrochim. Acta* **1996**, *41*, 641−651.
(47) Ren, B.; Li, X.-Q.; Wu, D.-Y.; Yao, J.-L.; Xie, Y.; Tian, Z.-Q. Orientational behavior of cyanide on a roughened platinum surface investigated by surface enhanced Raman spectroscopy. *Chem. Phys. Lett.* **2000**, *322*, 561−566.
(48) Shin, D. Spectroscopic evidence on the acetonitrile cleavage at mild condition. *Spectrochim. Acta, Part A* **2021**, *263*, 120191.
(49) Gu, R.; Cao, P.; Sun, Y.; Tian, Z. Surface-enhanced Raman spectroscopy studies of platinum surfaces in acetonitrile solutions. *J. Electroanal. Chem.* **2002**, *528*, 121−126.
(50) Dederichs, F.; Petukhova, A.; Daum, W. Adsorption of CN at the Pt(111)/liquid interface by dissociation of acetonitrile and the potentiality of CO contamination: A sum-frequency generation study. *J. Phys. Chem. B* **2001**, *105*, 5210−5216.
(51) Bozzini, B.; Fanigliulo, A. An in situ spectroelectrochemical Raman investigation of Au electrodeposition and electrodissolution in $KAu(CN)_2$ solution. *J. Appl. Electrochem.* **2002**, *32*, 1043−1048.
(52) Beltramo, G.; Shubina, T.; Mitchell, S.; Koper, M. Cyanide adsorption on gold electrodes: a combined surface enhanced Raman spectroscopy and density functional theory study. *J. Electroanal. Chem.* **2004**, *563*, 111−120.
(53) Briega-Martos, V.; Costa-Figueiredo, M.; Orts, J. M.; Rodes, A.; Koper, M. T.; Herrero, E.; Feliu, J. M. Acetonitrile adsorption on Pt single-crystal electrodes and its effect on oxygen reduction reaction in acidic and alkaline aqueous solutions. *J. Phys. Chem. C* **2019**, *123*, 2300−2313.
(54) Yang, G.; Ivanov, I. N.; Ruther, R. E.; Sacci, R. L.; Subjakova, V.; Hallinan, D. T.; Nanda, J. Electrolyte solvation structure at solid−liquid interface probed by nanogap surface-enhanced Raman spectroscopy. *ACS Nano* **2018**, *12*, 10159−10170.
(55) Peng, Z.; Freunberger, S. A.; Hardwick, L. J.; Chen, Y.; Giordani, V.; Bardé, F.; Novák, P.; Graham, D.; Tarascon, J. M.; Bruce, P. G. Oxygen reactions in a non-aqueous Li+ electrolyte. *Angew. Chem., Int. Ed.* **2011**, *50*, 6351−6355.
(56) Xu, C.; Ge, A.; Kannari, K.; Peng, B.; Xue, M.; Ding, B.; Inoue, K.-I.; Zhang, X.; Ye, S. The Decisive Role of Li_2O_2 Desorption for Oxygen Reduction Reaction in Li−O_2 Batteries. *ACS Energy Lett.* **2023**, *8*, 1289−1299.
(57) Reinsberg, P. H.; Baltruschat, H. Potential-and cation-dependent adsorption of acetonitrile on gold investigated via surface enhanced infrared absorption spectroscopy. *Electrochim. Acta* **2020**, *334*, 135609.

https://doi.org/10.1021/acs.jpcc.4c06709
J. Phys. Chem. C 2024, 128, 20148−20155